

A FALLING CORONA MODEL FOR THE ANOMALOUS BEHAVIOR OF THE BROAD EMISSION LINES IN NGC 5548

MOUYUAN SUN,^{1,2} YONGQUAN XUE,^{1,2} ZHENYI CAI,^{1,2} AND HENGXIAO GUO^{3,4}

¹*CAS Key Laboratory for Research in Galaxies and Cosmology, Department of Astronomy, University of Science and Technology of China, Hefei 230026, China; ericsun@ustc.edu.cn; xuey@ustc.edu.cn*

²*School of Astronomy and Space Science, University of Science and Technology of China, Hefei 230026, China*

³*National Center for Supercomputing Applications, University of Illinois at Urbana-Champaign, 605 East Springfield Avenue, Champaign, IL 61820, USA*

⁴*Department of Astronomy, University of Illinois at Urbana-Champaign, Urbana, IL 61801, USA*

(Revised **Draft: March 9, 2024**)

ABSTRACT

NGC 5548 has been intensively monitored by the AGN Space Telescope and Optical Reverberation Mapping collaboration. Approximately after half of the light curves, the correlation between the broad emission lines and the lag-corrected ultraviolet continua becomes weak. This anomalous behavior is accompanied by an increase of soft X-ray emission. We propose a simple model to understand this anomalous behavior, i.e., the corona might fall down, thereby increasing the covering fraction of the inner disk. Therefore, X-ray and extreme ultraviolet emission suffer from spectral variations. The ultraviolet continua variations are driven by both X-ray and extreme ultraviolet variations. Consequently, the spectral variability induced by the falling corona would dilute the correlation between the broad emission lines and the ultraviolet continua. Our model can explain many additional observational facts, including the dependence of the anomalous behavior on velocity and ionization energy. We also show that the time lag and correlation between the X-ray and the ultraviolet variations change as NGC 5548 displays the anomalous behavior. The time lag is dramatically longer than the expectation from disk reprocessing if the anomalous behavior is properly excluded. During the anomalous state, the time lag approaches the light-travel timescale of disk reprocessing albeit with a much weaker correlation. We speculate that the time lag in the normal state is caused by reprocessing of the broad line region gas. As NGC 5548 enters the abnormal state, the contribution of the broad line region gas is smaller; the time lag reflects disk reprocessing. We also discuss alternative scenarios.

Keywords: black hole physics-galaxies: active-galaxies: individual (NGC 5548)-quasars: emission lines

1. INTRODUCTION

Variations of active galactic nucleus (AGN) emission often provide model-independent constraints on the size of the emission region. This approach is particularly effective in studies of the cross correlation between two light curves of AGN emission. For instance, the cross correlation between the ultraviolet (UV) to optical variations of continua and broad emission lines (BELs) can probe the distance between the broad emission line region (BLR) and the ionizing continua (which is the extreme-UV, i.e., EUV, emission) and reveal the structure of the BLR. Similarly, the cross correlation between any two light curves of AGN continua can constrain the size of the central engine, which is widely believed to be powered by accretion of materials onto a supermassive black hole (SMBH).

Theoretically speaking, these correlations are causal in nature. The BLR is photoionized by the intense EUV photons and emits both high- (e.g., C IV) and low-ionization (e.g., H β) BELs. As a result, the BELs vary in response to the ionizing continuum variations after light-travel time delays. This is the “reverberation mapping” of BELs (RM; see Blandford & McKee 1982). This technique, which usually requires time-resolved spectroscopy, has been applied to some AGNs that are diverse in various properties (Kaspi et al. 2000, 2007; Peterson et al. 2002; Peterson 2014; Bentz et al. 2010b; Denney et al. 2010; Grier et al. 2012, 2017b; Du et al. 2014; Bentz & Katz 2015; Shen et al. 2016). Empirical relations between SMBH mass (M_{BH}) and the size and the velocity dispersion of the BLR have been established (which are calibrated by the scaling relations between SMBHs and the physical properties of the bulges of their host, see, e.g., Onken et al. 2004). These relations are referred as the single-epoch virial M_{BH} estimators (Vestergaard & Peterson 2006). Moreover, with high-quality RM data, it is possible to produce velocity-delay maps of BLR and constrain the kinematics of the BLR gas (e.g., Denney et al. 2009; Bentz et al. 2010a; Grier et al. 2012, 2017a).

The inter-band correlations and time lags might be explained by the X-ray reprocessing scenario (e.g., Krolik et al. 1991). In the model, the highly variable X-ray emission can illuminate and heat the surface layer of the outer accretion disk (for a review, see Reynolds & Nowak 2003). The surface layer then re-radiates the variable thermal emission that is at least partially responsible for the observed variations in UV, optical and near infrared (NIR) bands. Therefore, similar to that of the BLR case, the UV, optical and NIR emission follows the X-ray continuum variations after light-travel time delays. This model has been well developed and adopted to fit the multi-band light curves (e.g., Edelson et al. 1996, 2015, 2017; Wanders et al. 1997; Collier et al. 1998; Sergeev et al. 2005; McHardy et al. 2014, 2016, 2017; Shappee et al. 2014; Fausnaugh et al. 2016; Starkey et al. 2016; Cackett et al. 2017; Starkey et al. 2017; Pal & Naik 2018). It is found that the detected inter-band time lags are inconsistent with the classical thin disk theory (e.g., Fausnaugh et al. 2016; Starkey et al. 2017). Moreover, the time lag between X-ray

and UV emission is significantly longer than the light-travel timescale (e.g., Edelson et al. 2017; McHardy et al. 2017; but see McHardy et al. 2016). Other scenarios and characteristic timescales, e.g., the dynamical timescales, are proposed to explain the observations (e.g., Cai et al. 2017; Gardner & Done 2017).

NGC 5548, a well-studied RM AGN, has been frequently monitored by the most intensive RM experiment to date, the AGN Space Telescope and Optical Reverberation Mapping (STORM) collaboration. During this RM campaign, NGC 5548 was observed with space (including *Swift*, the *Hubble Space Telescope (HST)*; De Rosa et al. 2015; Edelson et al. 2015) and ground-based telescopes (Pei et al. 2017) with high cadence. The good time sampling, high signal-to-noise ratio (S/N), multiwavelength (including X-ray, UV, optical, and infrared) continua, and spectroscopic observations have guaranteed to explore the high degree of detail of the BLR (De Rosa et al. 2015; Pei et al. 2017), the accretion disk (Edelson et al. 2015; Fausnaugh et al. 2016), and the corona (Edelson et al. 2015).

As noted by Goad et al. (2016), the variations of BELs in NGC 5548 underwent an interesting and unexpected anomalous behavior. Approximately after half of the observations, the BELs and the UV continua varied almost independently. During this “abnormal” state, the X-ray spectra underwent a significant evolution (Mathur et al. 2017). The anomalous BEL variations infringe the basic RM assumptions and require a physical explanation. In this work, we propose a simple falling corona model, aiming to explain this transient anomalous phenomenon. We also illustrate that the abnormal state has an effect on the time lag measurements between X-ray and UV variations.

This paper is formatted as follows. In Section 2.1, we present the observational facts of the anomalous behavior in NGC 5548. In Section 2.2, we detail our simple model. We summarize our results in Section 4. In this work, we adopt $M_{\text{BH}} = 5 \times 10^7 M_{\odot}$ for NGC 5548 (Bentz & Katz 2015).

2. OBSERVATIONAL FACTS AND OUR MODEL

2.1. Observational facts

NGC 5548 was intensively monitored by the AGN STORM project. The time baseline of the campaign is ~ 180 days (i.e., between HJD=2,456,690 and HJD=2,456,866, or from 2014 February 1 through 2014 July 27). During the first half of the AGN STORM campaign, BELs and UV emission vary coherently. However, the coherence disappears starting on THJD ~ 6747 days (THJD=HJD−2,450,000) even if the mean flux is similar to that of the first half of the light curve (see Figure 1 of Goad et al. 2016 and Figure 7 of Pei et al. 2017). The observational constraints of the anomalous behavior in NGC 5548 are enumerated as follows (Goad et al. 2016; Mathur et al. 2017; Pei et al. 2017).

1. The response of the BELs to the UV continua behaves anomaly starting approximately midway through the campaign (Goad et al. 2016; Pei et al. 2017). To our surprise, the BELs and the UV continua are uncorre-

lated during this abnormal state. Meanwhile, the responsivity (i.e., the ratio of the changes of the BEL fluxes to the changes of the continuum) also decreases (i.e., the line emission is “lost”). Such anomalous behaviors are found for both high- (e.g., CIV) and low-ionization (e.g., H β) emission lines. The BLR structure cannot change in such a short timescale; the anomalous behaviors of BELs are likely caused by a depletion of EUV photons.

2. The fraction of emission line lost with respect to the UV fluxes, f_{lost} , is defined as $f_{\text{lost}} = 1 - f_{\text{obs}}/f_{\text{rec}}$, where f_{obs} and f_{rec} are the observed and the expected (which is reconstructed from the *HST* 1367 Å light curve; Goad et al. 2016) BEL fluxes, respectively. It is found that f_{lost} is distinctly velocity dependent. f_{lost} increases from the line center to the wings (see Figure 10 of Pei et al. 2017).
3. The fraction of line emission lost for the high-ionization BELs is higher than that of the low-ionization BELs. For instance, while the fraction of CIV lost is $\sim 18\%$, the fraction of H β lost is only $\sim 6\%$ (see Table 6 of Pei et al. 2017).
4. During the abnormal state, the fraction of soft X-ray excess increases (Mathur et al. 2017).
5. The abnormal state lasts for roughly ~ 50 days (Goad et al. 2016; Pei et al. 2017). NGC 5548 then returns to a normal state.

2.2. The model

We propose a simple falling corona model that is illustrated in Figure 1 to explain the observational facts listed in Section 2.1. The corona is radially extended (which is consistent with recent X-ray RM results; e.g., Wilkins et al. 2016) with a scale height equal to several times of the scale height of the accretion disk. The corona consists of two components, i.e., the upper optically thin and the lower optically thick layers. The former component produces power-law X-ray emission (e.g., Haardt & Maraschi 1993); the later component is responsible for the soft X-ray excess (e.g., Magdziarz et al. 1998). The formation of the corona is not entirely clear. For simplicity, we assume that the corona itself dissipates energy due to the viscous accretion process. That is, a substantial accretion power is released in the corona. The radiative efficiency of the corona is less than that of the disk.¹ Seed photons from the underlying thin disk (Shakura & Sunyaev 1973) are Compton up-scattered into X-ray photons.

In the normal state, the corona is speculated to be in quasi-equilibrium with the disk, i.e., there is no significant spectral

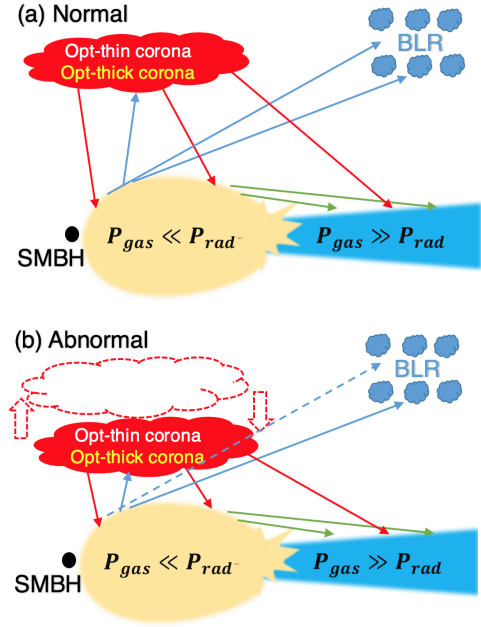


Figure 1. An illustration of our simple model. The X-ray corona consists of an optically-thick layer and an optically-thin component. The former Comptonizes the seed EUV photons from the inner disk (i.e., the blue solid light ray) and is responsible for the soft X-ray excess; the later up-scatters the comptonized continuum and emits the power-law X-ray emission. The X-ray emission also illuminates the underlying accretion disk (i.e., the red light rays). As the X-ray corona moves towards/away the accretion disk, NGC 5548 enters the abnormal state. This is because the fraction of the UV/EUV-emitting regions that are covered by the corona increases with the distance of the corona to the disk decreasing. As the corona moves closer to the accretion disk, more UV/EUV photons will be absorbed by the corona and up-scattered to X-rays. As such, the X-ray spectrum would be softer and the coherence between X-ray and UV photons would be diluted. The ionizing EUV photons seen by the BLR gas are then depleted (see the dashed light ray), resulting in flux lost in BELs. High-ionization ($E > 50$ eV) BELs and high-ionizing continuum are closer to the SMBH than their low-ionization counterparts and are more easily covered by the corona. Hence, high-ionization BELs (e.g., CIV) suffer deficits by a larger fraction than the low-ionization BELs (e.g., H β). The line wings are more likely produced in the inner parts of the BLR. As a result, the line-wing fluxes are depleted by a larger factor. As NGC 5548 exits to the abnormal state, the corona rises up to the original position. Note that the UV/EUV emission regions are expected to be radiation pressure dominated (see text).

variations. As pointed out by Rózańska et al. (2015), the optically thick (with optical depth > 5) corona component cannot exist in hydrostatic equilibrium with the accretion disk. Let us imagine that, due to thermal instabilities in the corona, the cooling is more efficient than the heating, and the corona will condense and thus fall down. This non-equilibrium process is responsible for the anomalous behavior in NGC 5548.

¹ As demonstrated by Meyer-Hofmeister & Meyer (1999) and Liu et al. (1999), the corona and the hot accretion flow (for a review, see Yuan & Narayan 2014) are similar in many aspects.

As the corona falls down, the covering fraction of the inner accretion disk increases. More seed photons emitted by the inner accretion disk will be inverse Compton up-scattered to X-rays. This leads to several observational consequences. First, spectral variations in the EUV to X-ray bands are expected, i.e., the spectrum will be softer. The variations of the normalization can lead to a positive inter-band correlation that drives the tight inter-band correlations in the normal state. On the contrary, the spectral variations can produce an anti-correlation between the seed and the up-scattered photons (e.g., EUV and X-ray). The observed variations in the X-ray or EUV bands are due to a combination of the variations of the normalization and spectral shape. As a result, the correlation between X-ray and EUV might be weak in the abnormal state. The UV variations could be driven by the X-ray and EUV variations. Hence, we expect weak correlation between EUV (BELs) and UV variations. Second, the fraction of EUV photons that ionize the BLR gas drops (e.g., the dashed light ray in Figure 1 is blocked) since the corona acts as a “shield” and up-scatters the EUV photons to X-ray ones. These two arguments can explain the observational facts #1 and #4.

In our scenario, the depletion of BEL fluxes depends mainly on the reduction of EUV photons and the change of the fraction of EUV photons directly seen by the BLR gas. As the corona falls down, the decreasing amplitude of the fraction of the EUV fluxes directly seen by the BLR gas is smaller for clouds with smaller opening angles (i.e., the ratio of the height to the radius, H/R). There is evidence that the BLR is anisotropic with $H/R < 1$ since the line profiles depend on inclination (e.g., Krolik 2001; Collin et al. 2006; Decarli et al. 2008; Runnoe et al. 2013; Shen & Ho 2014). The ratio H/R , as indicated by simple BLR kinematics modeling results (e.g., Kollatschny & Zetzl 2011), decreases with R . On the other hand, in some failed dusty wind BLR models (e.g., Baskin & Laor 2017), H/R scales with the dust opacity; the dust opacity increases with frequency. As R decreases, the accretion disk is hotter. That is, H/R is expected to decrease with increasing R . Therefore, the EUV photons that ionize the inner parts (i.e., smaller radii) of the BLR gas will be preferentially scattered by the corona as it falls down. Since the line wings are more likely produced in these regions, the fraction of emission line lost in the wings is larger than that of the line center (i.e., the observational fact #2). For NGC 5548, the shape of the velocity-resolved time-lag profile is roughly symmetric about the line center (Denney et al. 2009). Therefore, the blue and red wings show similar anomalous behaviors.

Compared with $H\beta$, high ionization emission lines (e.g., C IV) respond to the variations of high energy ionizing continuum. The emission region of the high ionizing continuum is much more compact and closer to the SMBH than the low ionizing one. It is therefore possible that, as the corona falls down, the high ionizing continuum is more preferentially up-scattered into soft X-rays than the low ionizing one. Meanwhile, the C IV gas is more closer to the SMBH than the $H\beta$ gas. Hence, the fractions of depletion fluxes of high ioniza-

tion emission lines are larger than those of low ionization emission lines. This can explain the observational fact #3.

As NGC 5548 returns to the normal state, we speculate that the corona rises up to the original position. The transition timescale between the normal and abnormal states is controlled by the cooling, the falling, and the Compton timescales of the corona. The falling timescale is simply the dynamical timescale, which is smaller than the thermal timescale (see Eq. 2). The Compton timescale of the corona with the seed photons generated in the classical thin accretion disk is (Ishibashi & Courvoisier 2012)

$$T_{\text{ct}} = \frac{3m_e c}{8\sigma_{\text{TC}}\mu} = 0.25 \frac{0.1}{\eta} \left(\frac{R_c}{100 R_S}\right)^2 \frac{0.1}{\dot{m}} \frac{M_{\text{BH}}}{5 \times 10^7 M_{\odot}} \frac{0.1}{\alpha} \text{ days} \quad (1)$$

where m_e , c , σ_{TC} , μ , R_c , R_S , η and \dot{m} are the mass of electron, the speed of light, the Thomson cross section, the photon energy density, the radial distance to the SMBH, the Schwarzschild radius, the radiative efficiency, and the ratio of the accretion rate to the Eddington accretion rate (i.e., $1.3 \times 10^{18} M_{\text{BH}}/M_{\odot} \text{ g s}^{-1}$), respectively.

For the corona with local viscous dissipation, the cooling time scale is (Cao 2016)

$$T_c = \frac{T_{\text{th}}}{f} = \frac{2\pi}{f\alpha\Omega_K} = 80 \left(\frac{R_c}{100 R_S}\right)^{\frac{3}{2}} \frac{M_{\text{BH}}}{5 \times 10^7 M_{\odot}} \frac{0.1}{\alpha f} \text{ days} \quad (2)$$

where T_c , T_{th} , α , and Ω_K are the cooling timescale, the thermal timescale, the dimensionless viscosity, and Keplerian angular velocity, respectively. $f < 1$ is the ratio of the radiation to the gravitational energy of the corona. It is evident that the cooling timescale is much longer than the dynamical and the Compton timescales. Hence, the transition timescale is mainly controlled by the cooling timescale, which is $T_c \sim 50/2 = 25$ days (i.e., the observational fact #5; the factor of 2 is introduced since NGC 5548 returns to the normal state). Therefore, the expected location of the corona is $R_c < 40 R_S$ (i.e., Eq. 2), which is extended enough to obscure the EUV emission regions. Note that the obscured disk should be radiation-pressure dominated (Shakura & Sunyaev 1973).

3. THE RELATION BETWEEN THE X-RAY AND UV VARIATIONS

3.1. Revisiting the cross correlation between X-ray and UV emissions

Motivated by the observational fact #4 and our model, we expect significant spectral evolution from the normal to the abnormal state. As discussed in Section 2.2, the observed X-ray variability could be driven by both the variations in the normalization and spectral shape. Therefore, its power spectral density might change as NGC 5548 moves from the normal to the abnormal states. The ICCFs (i.e., the interpolation cross-correlation function; see, e.g., Peterson et al. 1998) is depend on the power spectral density (PSD) of the light curves (Welsh 1999). Meanwhile, it is also speculated that the variable BLR diffuse continuum emission can bias

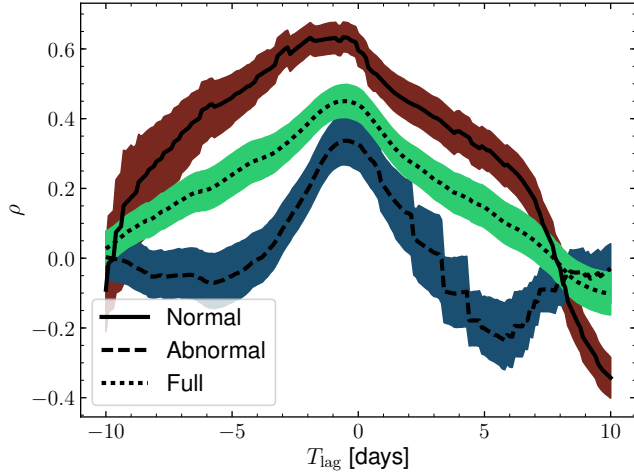


Figure 2. The ICCFs between the hard X-ray and the *HST* 1367 Å light curves. The solid, dashed, and dotted curves represent the ICCFs for the first segment (i.e., the normal state), the second segment (i.e., the abnormal state), and the full light curves, respectively. The shaded regions indicate the corresponding 1σ uncertainties (via the FR/RSS simulation). It is evident that the hard X-ray and the *HST* 1367 Å variations are tightly correlated during the normal state. This correlation is weak during the abnormal state. In Figures 2 & 3, we detrend the light curves by subtracting a 40-day boxcar running mean.

the time lag between the X-ray and UV variations. In the abnormal state, the BLR emission is suppressed. Therefore, the bias might be smaller than that of the normal state. Therefore, it is inappropriate to measure the time lag between X-ray and UV emission from the whole light curves. We therefore revisit the ICCF² between the X-ray and the *HST* 1367 Å light curves. Following Edelson et al. (2015) and Fausnaugh et al. (2016), we only interpolate the *HST* 1367 Å light curve and only consider the intensive monitoring period (i.e., from THJD= 6706 to 6831). We detrend the light curves by subtracting a 40-day boxcar running mean.

We separately apply the ICCF to the first (i.e., the normal state) and second (i.e., the abnormal state) segments of the light curves. The epoch separating the two segments is THJD= 6747 days (Pei et al. 2017).

The ICCFs for the hard X-ray (i.e., 0.8–10 keV) are shown in Figure 2. The uncertainties are estimated by performing the bootstrapping simulations (i.e., the FR/RSS; see Peterson et al. 1998). The correlation between the hard X-ray and the *HST* 1367 Å light curves is very tight in the normal state. On the contrary, the correlation is weak in the abnormal state.

We measure the centroids of the ICCFs in Figure 2. The centroid is calculated by considering the mean (weighted by the correlation coefficient ρ) time lag for $\rho > 0.8 \rho_{\max}$. Fig-

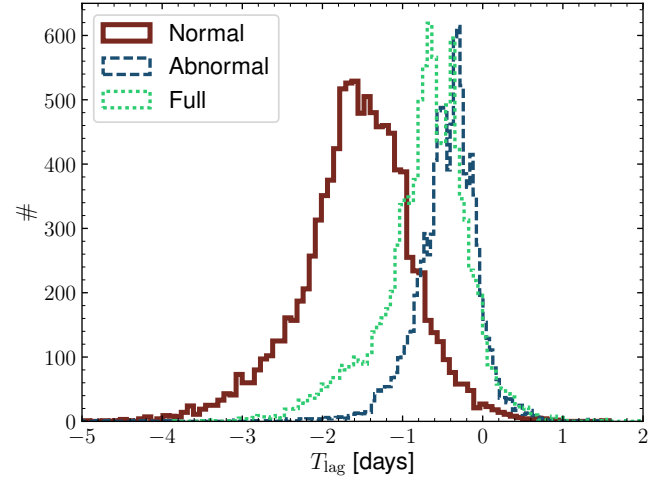


Figure 3. The observed-frame hard X-ray time lag distributions from our FR/RSS simulations. The solid, dashed, and dotted histograms represent the distributions of T_{lag} for the first segment (i.e., the normal state), the second segment (i.e., the abnormal state), and the full light curves, respectively. Negative values indicate that the hard X-ray leads the *HST* 1367 Å variations. The time lag in the abnormal state is shorter than that of the normal state. Therefore, the time lag is significantly underestimated if the full light curves were adopted.

ure 3 presents the distributions of the time lag of the hard X-ray with respect to the *HST* 1367 Å. If we only adopt the first segment (i.e., in the normal state), the time lag is $-1.54_{+0.44}^{-0.50}$ days in the observed frame, where the uncertainties correspond to the 25th and 75th percentiles of the distribution. This result is significantly larger than the time lag measured from the full light curves ($-0.65_{+0.28}^{-0.33}$ days). Therefore, the time lag reported in Edelson et al. (2015) is significantly biased by the second segment of the light curves. Interestingly, but not surprisingly, the time lag of the abnormal state is $-0.4_{+0.2}^{-0.25}$ days, which is shorter than the normal state.

These results would not be significantly changed if we measure the time lag by running *JAVLIN* (Zu et al. 2011). However, the time lag depends on the detrending timescales. Motivated by McHardy et al. (2017), we calculate the ICCFs and determine time lags for different detrending timescales, i.e., 5 days, 10 days, 20 days, 30 days, 40 days, and 60 days. The results for the normal state are presented in Figure 4. It is true that, for shorter smoothing timescales (e.g., 5 or 10 days), the time lag during the normal state tends to be smaller. However, the correlation between the hard X-ray and the *HST* 1367 Å light curve is also weaker. Moreover, the difference between the positive and negative peaks tend to diminish. Therefore, it is unclear whether the measured time lag for short smoothing timescales is robust. For the abnormal state, the ICCF properties (i.e., the time lag, the peak, and the difference between the positive and negative peaks) are largely independent from the smoothing timescale. If we

² We use PYCCF, Python Cross Correlation Function for reverberation mapping studies, to calculate the ICCFs. For details, see <http://ascl.net/code/v/1868>.

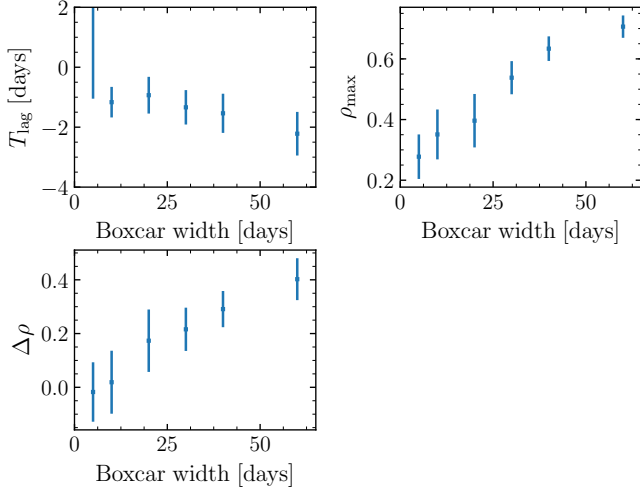


Figure 4. The relation between the ICCF properties and the smoothing timescale for the normal state. Upper left: The time lag between the hard X-ray and the *HST* 1367 Å light curves as a function of the boxcar smoothing timescale. Upper right: The ICCF peak as a function of the boxcar smoothing timescale. Lower left: The difference between the positive ICCF peak and the negative one as a function of the boxcar smoothing timescale. The time lag is indeed smaller if we adopted shorter boxcar smoothing timescales. However, the correlation tends to be weaker; the difference between the positive and negative peaks is also diminished.

consider the full light curves, the time lag and other ICCF properties approach those of the abnormal state.

We also explore the ICCFs between the soft X-ray (i.e., 0.3–0.8 keV) and the *HST* 1367 Å variations. We again find that the correlation of the normal state is significantly tighter than that of the abnormal state.

3.2. Comparison with previous works

The time lag between X-ray and UV emission is also explored in several other sources, e.g., NGC 2617 (Shappee et al. 2014), NGC 4151 (Edelson et al. 2017), NGC 4395 (McHardy et al. 2016) and NGC 4593 (McHardy et al. 2017). In these sources, the X-ray to UVW2 time lag is measured.

We have also estimated the time lag between the hard X-ray and UVW2 emission for the normal, the abnormal, and the full light curves of NGC 5548. For the full light curves, the time lag is $-1.13_{-0.3}^{+0.25}$ days, which is perfectly consistent with that of Edelson et al. (2015). However, if we divide the full light curve into two segments, the time lag changes. For the normal (abnormal) state, the time lag is $-3.08_{-0.48}^{+0.51}$ days ($-0.74_{-0.22}^{+0.18}$ days). Note that the time lag in the abnormal state agrees well with that of McHardy et al. (2014) who studied the *Swift* observations prior to the AGN STORM project. Therefore, like other sources (except for NGC 4395), the time lag of NGC 5548 in the normal state is vividly longer than the light-travel timescale of disk reprocessing (by a factor of ~ 10). However, the time lag of NGC 5548 in the

abnormal state again approaches the light-travel timescale albeit with a much weaker correlation.³

3.3. Implications to theoretical models

3.3.1. The implications of the time lag

We find that, after ignoring the second half of the AGN STORM light curves, the observed time lag between the hard X-ray and the *HST* 1367 Å emission is ~ 1.5 days (see Figure 3). The ~ 1.5 -day time lag is much longer than the light-travel timescale between the corona and the UV emission region (~ 0.2 days if the distance is $d \sim 40 R_S$). However, the time lag for the abnormal state is roughly consistent with the light-travel timescale (i.e., within $\sim 1 \sigma$ errorbar).

The observed change of the time lags from the normal to the abnormal state does not necessarily imply a mighty change of the distance between the corona and the UV emission regions. It could also be caused by other factors, e.g., the variation of the transfer function (i.e., the function that “translates” the X-ray light curves into UV light curves; see e.g., Eq. ~ 2 of Horne et al. 2004) or the PSDs. If so, we should also observe the changes in both the X-ray and UV structure functions (i.e., the function that describes the variability as a function of the separating timescale). We adopted the following definition to calculate the structure function (e.g., Sun et al. 2015),

$$\text{SF}(\Delta t) = \sqrt{(0.74\text{IQR}(\Delta m))^2 - \sigma_e^2} \quad (3)$$

where $\text{IQR}(\Delta m)$ is the 25% – 75% interquartile range of Δm and σ_e^2 is the median of the measurement variance of Δm . $\Delta m = -2.5 \log(f_2/f_1)$ is the difference between two observations (i.e., f_1 and f_2) separated by Δt . The constant 0.74 normalizes the IQR to be equivalent to the standard deviation of a Gaussian distribution.

The structure functions for the hard X-ray and the *HST* 1367 Å emission are presented in Figure 5. On timescales $\Delta t > 10$ days, NGC 5548 is evidently less variable in the abnormal state. The evolution of the structure function in hard X-ray is not unexpected in our simple falling corona model. As mentioned in Section 2.2, both normalization and spectral variations are expected during the abnormal state. The two types of variability may cancel each other, resulting weaker observed variations.

It is also interesting to mention that, for both two emission, the structure functions are more flat in the abnormal state, i.e., the contributions of short timescale (i.e., < 10 days) variations to the observed light curves are higher in the abnormal state than in the normal state. Therefore, our results appear to

³ We also explored the ICCFs between the hard X-ray and other UV-to-optical bands and obtained similar conclusions. The time lag in the normal state is much longer than the light-travel timescale of disk reprocessing; the time lag in the abnormal state approaches the light-travel timescale of disk reprocessing; the correlation in the abnormal state is much weaker than that of the normal state. Note that the properties of ICCFs between the *HST* 1367 Å and other UV-to-optical bands are not very sensitive to the anomalous behavior.

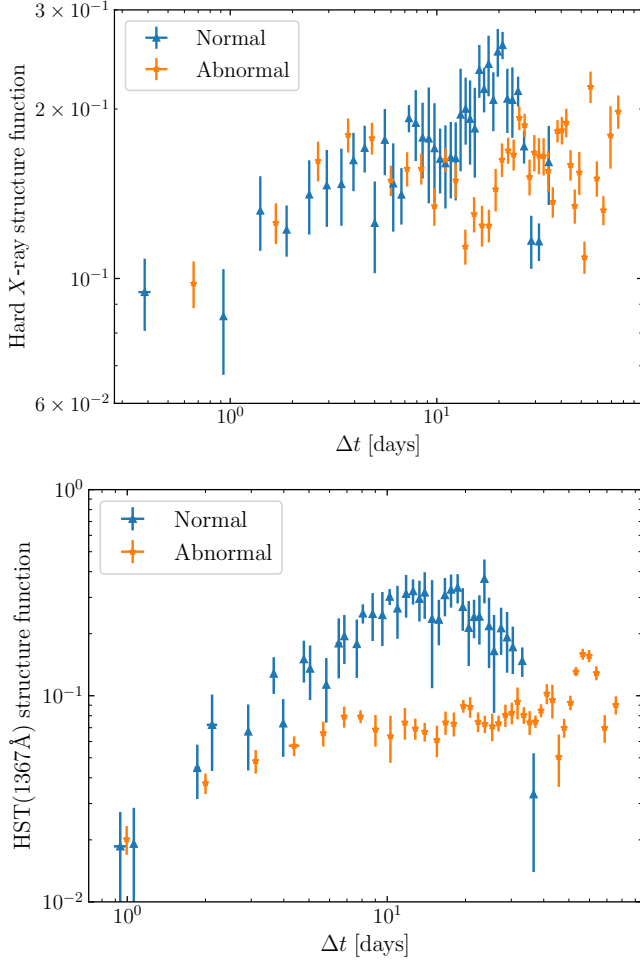


Figure 5. The structure functions for the hard X-ray (upper) and the HST 1367 Å emission (lower). On timescales $\Delta t > 10$ days, NGC 5548 is evidently more variable in the normal state. During the abnormal state, the structure functions are more flat implying higher contributions of short timescale variations to the observed light curves.

be consistent with the speculation that the time lag is consistent with the light-travel timescale of disk reprocessing if the long timescale variations are suppressed (see also McHardy et al. 2017).

How do we understand the time lags detected in the normal and abnormal states? There are several different scenarios. First, in addition to the accretion disk, there could be other reprocessors. For instance, as originally proposed by Korista & Goad (2001) and recently suggested by Cackett et al. (2017) and McHardy et al. (2017), the BLR gas might act as a second reprocessor. During the normal state, the contribution of the BLR component is strong; the observed ~ 1.5 -day time lag reflects the response of the BLR reprocessor (see, e.g., Figure 5 of Korista & Goad 2001). As NGC 5548 enters the abnormal state, the contribution of the BLR gas is weaker; the time lag approaches the light-travel timescale between the corona and the underlying disk. This speculation

is qualitatively consistent with the anomalous behavior of the BELs (i.e., the line emission is also “lost”) and our model. Meanwhile, unlike the disk reprocessing, the BLR component should contribute more to relatively long timescale variations. Hence, the variations of the HST 1367 Å emission on $\Delta t > 10$ days are suppressed in the abnormal state.

The second possibility is that the time lag is not related to the light-travel timescale. Cai et al. (2017) systematically explored the inter-band time lags by assuming a global common temperature fluctuation in the accretion disk. They further assumed that the timescale for the disk to respond to the global temperature fluctuations is radius-dependent (the timescale could be the dynamical or thermal timescale). They demonstrated that this phenomenological model has the potential to explain the observed time lags among UV-to-IR bands. If we assume that the corona varies in lockstep with the innermost (i.e., $< 15 R_S$) accretion disk, we can also calculate the predicted time lag between the hard X-ray and the HST 1367 Å emission from the Cai et al. (2017) model. We find that the predicted time lag is $-2.69_{+0.5}^{-0.73}$ days that is roughly consistent with the time lag in the normal state. It is worth noting that, if the size of the corona increases, the difference between the timescale of the corona respond to the global temperature fluctuations and that of the UV emission decreases. As a result, the time lag can be smaller.

The third possibility is that, as speculated by Gardner & Done (2017), the dynamical or thermal timescales might be responsible for the observed inter-band time lags. We can then estimate the radius of the HST 1367 Å emission region by assuming that the observed 1.5-day time lag is related to the dynamical timescale. We find that the required radius is $R_{rp} \sim 40 R_S$ which is quite consistent with the expectation of the accretion theory (Fausnaugh et al. 2016). This scenario, however, has the difficulty to explain the short time lag in the abnormal state unless the dynamical or thermal timescale is somehow not important in the abnormal state.

3.3.2. The implications of the correlation coefficient

As we mentioned in Section 3.1 (and Figure 2), the correlation between the hard X-ray and the UV emission is rather tight if we ignore the second half of the light curves (i.e., the abnormal light curves). Indeed, the maximum correlation coefficient $\rho_{\max} = 0.62 \pm 0.04$. We also use the lag-corrected HST 1367 Å light curve to reconstruct the associated X-ray emission. First, we fitted the *continuous time first-order autoregressive process* (i.e., CAR(1); see, e.g., Kelly et al. 2009) to the lag-corrected HST 1367 Å light curve (a 40-day boxcar running mean is subtracted) using *CARMA*⁴ (Kelly et al. 2014). Second, we adopted the best-fitting CAR(1) model to simulate the HST 1367 Å flux associated with the hard X-ray flux (a 40-day boxcar running mean is also subtracted) at each epoch. Third, we fitted a linear relation to the first half (i.e., THJD < 6747 days) of two light curves.

⁴ This package can be downloaded from https://github.com/brandonckelly/carma_pack.

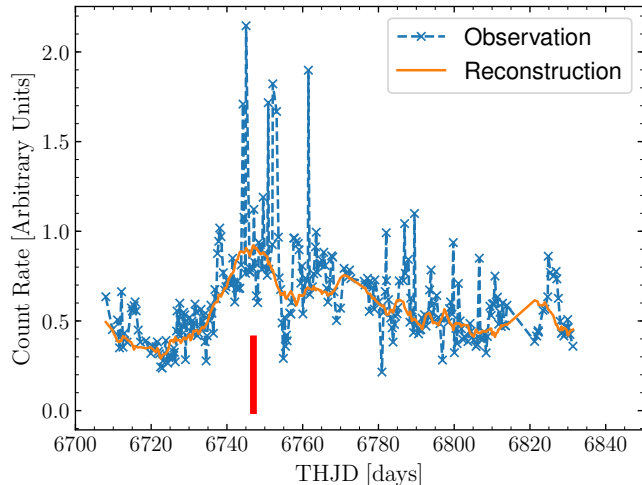


Figure 6. A comparison between the observed (a 40-day boxcar running mean is subtracted) and reconstructed hard X-ray light curves. For $\text{THJD} < 6747$ (i.e., the “normal” state), the two light curves are well matched. A similar correlation is not observed in the “abnormal” state. The red thick vertical line indicates $\text{THJD} = 6747$ days.

Each data point is weighted by its measurement error. Using the best-fitting linear relation and the simulated HST 1367 Å flux, we reconstructed the hard X-ray flux. In Figure 6, we present both the observed and reconstructed hard X-ray light curves. For $\text{THJD} < 6747$ days, the two light curves are reasonably matched. The tight correlation between the X-ray and UV emission is also observed for another source, NGC 4593 (McHardy et al. 2017).

During the abnormal state, the correlation between the hard X-ray and the HST 1367 Å emission is rather poor ($\rho_{\text{max}} = 0.34$). There are “outliers” in the hard X-ray light curve, i.e., the count rate increases by a factor of > 2 within a few days. Similar features are not observed in the HST 1367 Å light curve. However, it should be noted that the poor correlation is not caused by these outliers. We tried to remove these X-ray outliers and recalculated the ICCF of the abnormal state. The maximum correlation coefficient $\rho_{\text{max}} = 0.36$, i.e., the correlation is still poor.

How do we understand the change of the correlation coefficient? For instance, according to our falling corona model, the UV variations can be driven by both the X-ray fluctuations and the changes of the solid angle subtended by the UV emission regions from the corona. Meanwhile, the time lag of the abnormal state is small. The ICCF depends more critically on the interpolation since the sampling interval is larger than the observed time lag. Therefore, the correlation between the X-ray and UV variations is diluted.

Gardner & Done (2017) explored the expected correlation between the hard X-ray and the UV emission from the X-ray reprocessing scenario. They found that the simulated correlation is much tighter than the AGN STORM light curves and concluded that the observed UV-optical variations are

unlikely driven by the X-ray variability. Instead, they proposed that the hot X-ray corona cannot directly illuminate the accretion disk that is shielded by a UV torus. The X-ray emission heats the UV torus; the UV torus then illuminates the underlying accretion disk. As X-ray emission varies, a heating wave dissipates outwards, which drives the variability of the disk emission (e.g., optical emission). That is, the variability of long-wavelength (i.e., optical, IR) emission is controlled by the UV torus rather than the corona. Therefore, the correlation between the hard X-ray and UV emission can be poor. This model seems to be able to explain the poor correlation in the abnormal state. However, in the normal state, $\rho_{\text{max}} = 0.62$ (if we interpolate the hard X-ray light curve, then $\rho_{\text{max}} = 0.81 \pm 0.05$) is not radically smaller than the expectation of the simple X-ray reprocessing (the simulated $\rho_{\text{max}} \cong 0.8 \sim 0.9$; see Figures 4 & 5 of Gardner & Done 2017). Hence, the UV torus appears to be weak or absent in the normal state.

The weak correlation between the X-ray and the UV variations is also observed in another source NGC 4151 (Edelson et al. 2017). However, it is quite possible that the observed X-ray emission does not vary in phase with the one that illuminates the accretion disk. For instance, gas clouds can move into/away from light of sight on short timescales (for NGC 4151, see Wang et al. 2010). Therefore, the nature of the weak correlation could be different from that of the abnormal state of NGC 5548.

4. SUMMARY

We propose a simple falling corona model to explain the anomalous behavior of the broad emission lines in NGC 5548. In our model, NGC 5548 enters the abnormal state as the corona falls down towards the accretion disk. During this process, the covering factor of the corona increases. This process can naturally explain the observational facts summarized in Section 2.1.

We demonstrate that the time lag between X-ray and UV emission reported in the previous work is biased due to the anomalous behavior. The time lag in the normal state is $-1.54_{-0.50}^{+0.44}$ days (in the observed frame). The light-travel time delay cannot account for the ~ 1.5 -day time lag. As NGC 5548 enters the abnormal state, the time lag approaches the light-travel timescale between the corona and the accretion disk. We speculate that the time lag in the normal state is related to reprocessing from the BLR gas. As NGC 5548 enters the abnormal state, the BLR contribution is smaller. Therefore, the time lag reflects disk reprocessing. However, other possibilities can not be excluded.

We also show that the correlation between the hard X-ray and UV variations can be tight ($\rho_{\text{max}} \sim 0.6$) if the anomalous behavior is properly excluded. The correlation coefficient is roughly consistent with the simple X-ray reprocessing scenario. Therefore, the UV torus component proposed by Gardner & Done (2017) is weak or absent in the normal state of NGC 5548.

Our model makes a clear prediction. Instead of falling down, the corona can also rise up to a larger scale of height.

During the rising process, another type of the anomalous behavior of the BELs occurs. That is, while the correlation between the variations of quasar continua and BELs is destroyed, the BELs also show excess fluxes (i.e., $f_{\text{lost}} < 0$) than the reconstructed BEL light curves (e.g., from the *HST* 1367 Å light curve) and the X-ray spectrum is harder. Future RM experiments can verify such a scenario.

We acknowledge Prof. Wei-Min Gu and Prof. Jun-Xian Wang for beneficial discussion. M.Y.S. and Y.Q.X. acknowledge the support from NSFC-11603022, NSFC-11473026,

NSFC-11421303, the 973 Program (2015CB857004), the China Postdoctoral Science Foundation (2016M600485), the CAS Frontier Science Key Research Program (QYZDJ-SSW-SLH006), and the Fundamental Research Funds for the Central Universities. Z.Y.C. acknowledges the support from NSFC-11503024.

Software: Astropy (Astropy Collaboration et al. 2013), CARMA (Kelly et al. 2014), Matplotlib (Hunter 2007), Numpy & Scipy (Van Der Walt et al. 2011), PYCCF (Sun et al. 2018)

REFERENCES

- Astropy Collaboration, Robitaille, T. P., Tollerud, E. J., et al. 2013, *A&A*, 558, A33
- Baskin, A., & Laor, A. 2017, arXiv:1711.00025
- Bentz, M. C., Horne, K., Barth, A. J., et al. 2010a, *ApJL*, 720, L46
- Bentz, M. C., & Katz, S. 2015, *PASP*, 127, 67
- Bentz, M. C., Walsh, J. L., Barth, A. J., et al. 2010b, *ApJ*, 716, 993
- Blandford, R. D., & McKee, C. F. 1982, *ApJ*, 255, 419
- Cackett, E. M., Chiang, C.-Y., McHardy, I., et al. 2017, arXiv:1712.04025
- Cai, Z.-Y., Wang, J.-X., Zhu, F.-F., et al. 2017, arXiv:1711.06266
- Cao, X. 2016, *ApJ*, 817, 71
- Collier, S. J., Horne, K., Kaspi, S., et al. 1998, *ApJ*, 500, 162
- Collin, S., Kawaguchi, T., Peterson, B. M., & Vestergaard, M. 2006, *A&A*, 456, 75
- Decarli, R., Labita, M., Treves, A., & Falomo, R. 2008, *MNRAS*, 387, 1237
- Denney, K. D., Peterson, B. M., Pogge, R. W., et al. 2009, *ApJL*, 704, L80
- Denney, K. D., Peterson, B. M., Pogge, R. W., et al. 2010, *ApJ*, 721, 715
- De Rosa, G., Peterson, B. M., Ely, J., et al. 2015, *ApJ*, 806, 128
- Du, P., Hu, C., Lu, K.-X., et al. 2014, *ApJ*, 782, 45
- Edelson, R. A., Alexander, T., Crenshaw, D. M., et al. 1996, *ApJ*, 470, 364
- Edelson, R., Gelbord, J., Cackett, E., et al. 2017, *ApJ*, 840, 41
- Edelson, R., Gelbord, J. M., Horne, K., et al. 2015, *ApJ*, 806, 129
- Fausnaugh, M. M., Denney, K. D., Barth, A. J., et al. 2016, *ApJ*, 821, 56
- Gardner, E., & Done, C. 2017, *MNRAS*, 470, 3591
- Goad, M. R., Korista, K. T., De Rosa, G., et al. 2016, *ApJ*, 824, 11
- Grier, C. J., Peterson, B. M., Pogge, R. W., et al. 2012, *ApJ*, 755, 60
- Grier, C. J., Pancoast, A., Barth, A. J., et al. 2017a, *ApJ*, 849, 146
- Grier, C. J., Trump, J. R., Shen, Y., et al. 2017b, *ApJ*, 851, 21
- Haardt, F., & Maraschi, L. 1993, *ApJ*, 413, 507
- Horne, K., Peterson, B. M., Collier, S. J., & Netzer, H. 2004, *PASP*, 116, 465
- Hunter, J. D. 2007, *Computing in Science and Engineering*, 9, 90
- Ishibashi, W., & Courvoisier, T. J.-L. 2012, *A&A*, 540, L2
- Kaspi, S., Smith, P. S., Netzer, H., et al. 2000, *ApJ*, 533, 631
- Kaspi, S., Brandt, W. N., Maoz, D., et al. 2007, *ApJ*, 659, 997
- Kelly, B. C., Bechtold, J., & Siemiginowska, A. 2009, *ApJ*, 698, 895-910
- Kelly, B. C., Becker, A. C., Sobolewska, M., Siemiginowska, A., & Uttley, P. 2014, *ApJ*, 788, 33
- Korista, K. T., & Goad, M. R. 2001, *ApJ*, 553, 695
- Krolik, J. H., Horne, K., Kallman, T. R., et al. 1991, *ApJ*, 371, 541
- Krolik, J. H. 2001, *ApJ*, 551, 72
- Kollatschny, W., & Zetzl, M. 2011, *Nature*, 470, 366
- Liu, B. F., Yuan, W., Meyer, F., Meyer-Hofmeister, E., & Xie, G. Z. 1999, *ApJL*, 527, L17
- Magdziarz, P., Blaes, O. M., Zdziarski, A. A., Johnson, W. N., & Smith, D. A. 1998, *MNRAS*, 301, 179
- Mathur, S., Gupta, A., Page, K., et al. 2017, *ApJ*, 846, 55
- Meyer-Hofmeister, E., & Meyer, F. 1999, *A&A*, 348, 154
- McHardy, I. M., Cameron, D. T., Dwelly, T., et al. 2014, *MNRAS*, 444, 1469
- McHardy, I., Connolly, S., Cackett, K. E., et al. 2017, arXiv:1712.04852
- McHardy, I. M., Connolly, S. D., Peterson, B. M., et al. 2016, *Astronomische Nachrichten*, 337, 500
- Onken, C. A., Ferrarese, L., Merritt, D., et al. 2004, *ApJ*, 615, 645
- Pal, M., & Naik, S. 2018, *MNRAS*, 474, 5351
- Pei, L., Fausnaugh, M. M., Barth, A. J., et al. 2017, *ApJ*, 837, 131
- Peterson, B. M., Berlind, P., Bertram, R., et al. 2002, *ApJ*, 581, 197
- Peterson, B. M., Wanders, I., Horne, K., et al. 1998, *PASP*, 110, 660
- Peterson, B. M. 2014, *SSRv*, 183, 253
- Reynolds, C. S., & Nowak, M. A. 2003, *PhR*, 377, 389
- Rózańska, A., Malzac, J., Belmont, R., Czerny, B., & Petrucci, P.-O. 2015, *A&A*, 580, A77
- Runnoe, J. C., Brotherton, M. S., Shang, Z., Wills, B. J., & DiPompeo, M. A. 2013, *MNRAS*, 429, 135
- Sergeev, S. G., Doroshenko, V. T., Golubinskiy, Y. V., Merkulova, N. I., & Sergeeva, E. A. 2005, *ApJ*, 622, 129

- Shakura, N. I., & Sunyaev, R. A. 1973, *A&A*, 24, 337
- Shappee, B. J., Prieto, J. L., Grupe, D., et al. 2014, *ApJ*, 788, 48
- Shen, Y., & Ho, L. C. 2014, *Nature*, 513, 210
- Shen, Y., Horne, K., Grier, C. J., et al. 2016, *ApJ*, 818, 30
- Starkey, D., Horne, K., Fausnaugh, M. M., et al. 2017, *ApJ*, 835, 65
- Starkey, D. A., Horne, K., & Villforth, C. 2016, *MNRAS*, 456, 1960
- Sun, M., Grier, C. J., Peterson, B. M. 2018, *PYCCF*, <https://ascl.net/code/v/1868>
- Sun, M., Trump, J. R., Shen, Y., et al. 2015, *ApJ*, 811, 42
- Van Der Walt, S., Colbert, S. C., & Varoquaux, G. 2011, arXiv:1102.1523
- Vestergaard, M., & Peterson, B. M. 2006, *ApJ*, 641, 689
- Wanders, I., Peterson, B. M., Alloin, D., et al. 1997, *ApJS*, 113, 69
- Wang, J., Risaliti, G., Fabbiano, G., et al. 2010, *ApJ*, 714, 1497
- Welsh, W. F. 1999, *PASP*, 111, 1347
- Wilkins, D. R., Cackett, E. M., Fabian, A. C., & Reynolds, C. S. 2016, *MNRAS*, 458, 200
- Yuan, F., & Narayan, R. 2014, *ARA&A*, 52, 529
- Zu, Y., Kochanek, C. S., & Peterson, B. M. 2011, *ApJ*, 735, 80